A Single Picture Explains Diversity of Hyperthermia Response of Magnetic Nanoparticles

Ivan Conde-Leboran,[,1] Daniel Baldomir,[1] Carlos Martinez-Boubeta,[2] Oksana Chubykalo-Fesenko,[3] María del Puerto Morales,[3] Gorka Salas,[3,4] David Cabrera,[4] Julio Camarero,[4,5] Francisco J. Teran,[4,6] and David Serantes*[,3]*

[1]Instituto de Investigacións Tecnolóxicas, and Departamento de Física Aplicada, Universidade de Santiago de Compostela, 15782 Santiago de Compostela, Spain

[2] CMB is a freelancer in Santiago de Compostela, Spain. This work was partly completed while he was a researcher at Barcelona University

[3]Instituto de Ciencia de Materiales de Madrid, CSIC, Cantoblanco, ES-28049 Madrid, Spain

[4]IMDEA Nanociencia, Campus Universitario de Cantoblanco, 28049 Madrid, Spain

[5]Dpto. Física de la Materia Condensada, and Instituto Nicolas Cabrera, Universidad Autónoma de Madrid, Campus Universitario de Cantoblanco, 28049 Madrid, Spain

[6]Unidad Asociada de Nanobiotecnología CNB-CSIC & IMDEA Nanociencia, Campus Universitario de Cantoblanco, 28049 Madrid, Spain

E-mail: ivan.conde@usc.es, david.serantes@icmm.csic.es

ABSTRACT

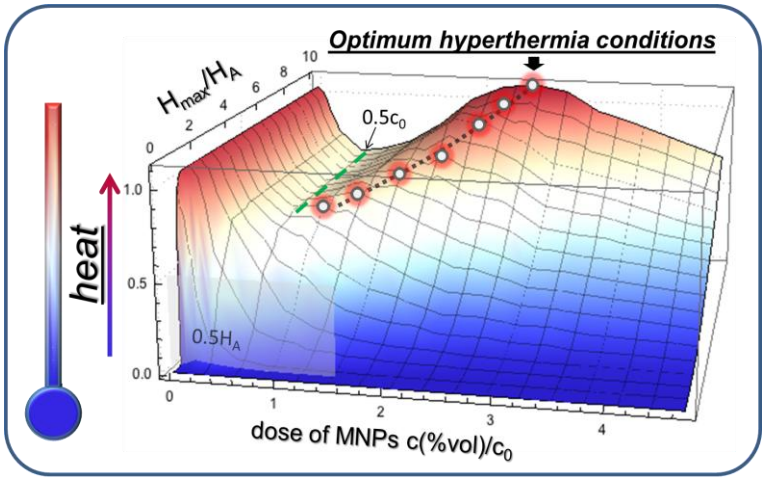

Progress in the design of nanoscale magnets for localized hyperthermia cancer therapy has been largely driven by trial-and-error approaches, for instance, by changing of the stoichiometry composition, size, and shape of the magnetic entities. So far, widely different and often conflicting heat dissipation results have been reported, particularly as a function of the nanoparticle concentration. Thus, achieving hyperthermia-efficient magnetic ferrofluids remains an outstanding challenge. Here we demonstrate that diverging heat-dissipation patterns found in the literature can be actually described by a single picture accounting for both, the intrinsic magnetic features of the particles (anisotropy, magnetization) and experimental conditions (concentration, magnetic field). Importantly, this general magnetic-hyperthermia scenario also predicts a novel non-monotonic concentration dependence with optimum heating features, which we experimentally confirmed in iron oxide nanoparticle ferrofluids by fine-tuning the particle size. Overall, our approach implies a *magnetic hyperthermia trilemma* that may constitute a simple strategy for development of magnetic nanomaterials for optimal hyperthermia efficiency.

KEYWORDS: Magnetic nanoparticles; Dipolar interactions; Hyperthermia; Monte Carlo

The possibility of treating tumors with magnetic nanoparticles has produced much excitement in recent years because it paves the way for new therapeutic methods which can be controlled by external means.[1] In addition, novel advances in chemistry have allowed bioconjugated magnetic particles to be specifically targeted to cancer cells; hence the development of 'personalized and tailored drugs' within the Ehrlich's magic bullet paradigm becomes a possibility.[2] In this new scenario, magnetic-fluid hyperthermia (i.e. heating with magnetic nanoparticles under an external AC field, H_{AC}) holds great promise for the treatment of cancer.[3] It conjugates deep tissue penetration with fine spatial resolution to destroy[4] or enhance the drug sensitivity[5] of the malignant cells by heating. Therefore more specificity and efficacy are foreseen over traditional cancer treatments including surgery, radiation therapy and pharmacology; advantages all together fostering the great interest and research efforts devoted to the topic in the last years (see Ref. [6] and references therein).

However, further improvement is still needed before hyperthermia can become a standard medical procedure. In particular, the first goal is maximizing the electromagnetic-into-heat energy conversion in order to reduce the amount of particles in therapy. To this end, the heating performance of a plethora of magnetic particles has been examined under different experimental conditions; the roles of particle size and composition, and its dependence on the frequency and amplitude of the applied magnetic field have been studied in detail.[7] Besides, understanding efficiency and dose–response hyperthermia relationship is crucial when it comes to clinical translation.[1] However, and this is perhaps the main issue for concern, data from studies in the literature show enormous discrepancy in the heating performance as a function of particle

concentration –i.e. dose-, ranging from a detrimental influence of concentration on the heating power of the particles, to even the opposite (see e.g. Refs. [8, 9, 10, 11, 12]). Furthermore, changes on those tendencies can be observed for the same system depending on the H_{AC} as well. Therefore, a central milestone in the magnetic-fluid hyperthermia roadmap is to unveil the physical scenario able to explain the large variety of hyperthermia responses reported in the literature.

Here we aim to shed some light into this complex issue, and to provide the right setting for the understanding of the heating performance of nanoparticle systems as a function of both the particle concentration (*c*), i.e., comparable to the clinical dose, and the amplitude of the applied field (H_{MAX}). Contrary to the assumptions made in some simplified calculations here we consider that magnetic particles interact with each other,[13,14] and this interaction inevitably influences the heating efficiency.[15,16,17] In the following we build a unified picture accounting for the heating performance of magnetic nanoparticle systems, demonstrating that apparently different hyperthermia trends reported in the literature can in fact be understood as particular regions within this general magnetic-hyperthermia scenario.

Results and Discussion

Magnetic Modeling. Assessing the heating capability of particles exposed to an alternating magnetic field, i.e. the *Specific Absorption Rate* (SAR), is equivalent to evaluate the hysteresis losses (HL) per cycle,[6] since $SAR=HL \cdot f$, being f the frequency of the external AC magnetic field. In this study we use a Monte Carlo model to simulate hysteresis loops under different experimental conditions, to theoretically derive the HL as the area of the hysteresis loops for a freely (non-aggregated) collection of nanoparticles (for an insight into the role of aggregation see e.g. Ref. [18]). We consider an idealized collection of monodisperse single-domain

ferro(i)magnetic particles characterized by their K, M_S and V; being those the effective magnetic anisotropy constant, saturation magnetization and volume of the particles, respectively. For the sake of simplicity we consider that the size of the particles is large enough so that the particles behave ferromagnetic-like, i.e. superparamagnetic –dissipationless- behavior is avoided (see section *Computational details* in **Methods**). To illustrate the key ingredient of our approach, we show in Figure 1 some M(H) hysteresis curves under different field amplitude and interaction conditions. Please note, renormalization of the results in units of $H_A = 2K/M_S$, the anisotropy field, makes our analysis independent of the specific sample characteristics (i.e. K and M_S values), and hence suitable for any system fulfilling the conditions assumed within the model. Likewise, for the sake of universality we introduce also a dimensionless ratio $c_0 = 2K/M_S^2$ for normalizing the influence of the dipolar interactions, which interaction is modulated by changing the sample concentration *c*. The c_0 value weights the relative importance between the anisotropy (proportional to K) and dipolar (proportional to M_S^2) energies,[14] and normalizes the influence of dipolar interactions in the same way as H_A weights the importance of the field amplitude, H_{MAX}.

The results shown in Fig. 1 demonstrate that large differences on the hysteresis area correlate with both H_{MAX} and *c*. On one hand, minor hysteresis loops are observed for all concentrations at low-field amplitudes ($H_{MAX}/H_A < 0.5$) as shown in Fig. 1(a). On the other hand, considerable hysteresis appears above the 0.5 ratio (which roughly corresponds to coercive field in the non-interacting case) but drops rapidly with increasing *c*, as depicted in Fig. 1(b). Larger fields ($H_{MAX}/H_A \geq 1.0$) allow for larger hysteresis loops at higher concentrations, as shown in Fig. 1(c,d). A careful choice of H_{MAX} and *c* is therefore needed in order to have an efficient hyperthermia performance.

Conflicting requirements – *magnetic hyperthermia trilemma*. As mentioned above, the heating power SAR is defined as energy per cycle times frequency (*f*); thus, by having both large HL and *f* would ideally be possible to achieve very large SAR values. However, when it comes to clinical applications the maximum H_{MAX} and f values are quite limited, due to the technical challenge of generating large alternating magnetic fields over large volumes as that of a human body.[19] If focusing on the case of frequencies large enough as to avoid superparamagnetic behavior (hundreds of kHz), H_{MAX} is limited in practice to several hundreds of Oe, of the order of the anisotropy field of common particles in hyperthermia experiments. We have seen that the HL can be negligible if the ratio H_{MAX}~$0.5H_A$ is not surpassed, hence it will be crucial to choose the particles so that their characterizing K and M_S parameters allow obtaining relevant HL for the experimentally achievable H_{MAX}. But as we have seen in Fig. 1, also the role of interparticle interactions needs to be considered.

Firstly, please note that the magnetic hysteresis losses scale (for non-interacting conditions) approximately as HL ≈ 2K.[20,21,22] Therefore, increasing the K of the particles would lead to an increase of the SAR. Regarding the latter, the tuning of the magnetocrystalline anisotropy and its influence on magnetic heating efficiency was already discussed by Lee *et al.*[23] The previous statement could mislead us to the idea that the best particles are those with higher K. But the large anisotropy also implies that very large fields are required to switch the particles' magnetization orientation (please keep in mind that $H_A = 2K/M_S$). As a result, the magnetization can no longer be switched with in-clinic available fields, and the obtainable hysteresis losses remain limited. Alternatively, the anisotropy energy barrier (KV) can be tuned through the desired range by setting the volume of the particles (V) accordingly, so that for smaller K, the volume should be proportionally increased (while avoiding sizes beyond the multidomain

transition, with much smaller heating performance). Still, larger V increases the interparticle dipolar interactions -which are proportional to $(M_S V)^2$-, that significantly increase the saturation field and thus modify the hyperthermia performance in a complex nontrivial way.[14] A similar drawback results from increasing the saturation magnetization M_S: despite it might help decreasing the required H_{MAX} to attain relevant HL values since larger M_S diminishes H_A, the higher M_S leads also to stronger interparticle dipolar interactions. Note that power issues associated with poor SAR values are nowadays circumvented by increasing the concentration of material,[24] which again, would boost dipolar interactions. Because both strategies have advantages and disadvantages, it is the best to use a combination.

In view of the above it is apparent that, when it comes to heat dissipation, the different ingredients determining the heating response (i.e. type of particles -characterized by K, M_S, and V-; AC field; and sample concentration), constitute conflicting requirements that must be therefore simultaneously considered in order to obtain a desired heat release. Thus, similarly to the problems encountered in magnetic recording,[25] we can summarize those intimately entwined ingredients in a *magnetic hyperthermia trilemma*, as illustrated in Fig. 2.

A general magnetic-hyperthermia scenario. Next we show how the complex heating scenario corresponding to the *magnetic hyperthermia trilemma* can be accounted by a single picture (Figure 3) as a function of both H_{MAX} and *c*, and where different types of particles are translated into this picture through their characteristic K and M_S values. Overall, the results show a drastic influence of the volume concentration on the heating properties depending on H_{MAX}, with completely different features expected for different combinations of K and M_S. In brief, particles with large K and small M_S (i.e. both H_A and c_0 are large) will be limited to small c/c_0 values and the typical experimental H_{MAX}/H_A ratios will mostly correspond to the low-field

curves. Contrarily, small K and large M_S (therefore, small H_A and c_0) stand for a broad range of c/c_0 values and correspond to large H_{MAX}/H_A curves. For intermediate K and M_S values we can expect a variety of responses depending on their magnitudes and experimental conditions. Thus, what is depicted in Fig. 3 is a *general picture able to explain completely different heating behaviors depending both on the features of the particles and specific experimental conditions*. To check the feasibility of our model, we next benchmark it against a diversity of experimental results reported in the literature.

Comparison to examples given in the literature. In most cases, a decrease of the heating efficiency (HL/2K) with increasing ferrofluid concentration (c/c_o) is observed, as illustrated in Fig. 4(a), while the opposite trend corresponding to Fig. 4(b) is rarely observed. Nevertheless, increased SAR that resulted from the particle dipole interaction in soft ferrites can be found in (figure within) Jeun *et al*.[26] In Fig. 4(c), the field-dependence of the heating efficiency is analyzed for different concentrations. Increasing heating at low magnetic field requires the decrease of nanoparticle anisotropy (lower c_0), this figure bear similarities to the work by Khot *et al*.[27] It is worth to mention here that sometimes, it is misguidedly assumed in the literature a square dependence on the magnetic field, which results from linear approximation theories.[6] Similarly to our case, departure from the quadratic dependence of SAR on the H_{MAX} can be found also in Beković *et al*.[28] A comprehensive discussion can be found in a recent paper by Landi and Bakuzis,[29] and it is also beautifully illustrated in (figure 8 within) Ref. [30]. In addition, Fig. 4(d) shows the concentration-dependence of the heating efficiency at different field conditions, which compares to the results reported in (figure 5 within) Cervadoro *et al*.[31] We note in Fig. 4(e) an enhancement of the heating capabilities on increasing the anisotropy constant (herein M_S = 420 emu/cm^3; sample concentration c = 0.1), akin to the report by Lee *et al*. on

exchange-coupled magnetic particles.[23] Fig. 4(f) depicts the evolution of the heating capabilities as a function of magnetic field for different saturation magnetizations (here, K = 50000 erg/cm^3; c = 0.1), mimicking the results reported by Chaudret and co-workers.[32] An increasing behavior of SAR values against M_S is also plotted in (figure 13 within) Sousa *et al*.[33] A similar dependence of the heating power on the evolution of the saturation magnetization has been recently reported by Lartigue *et al*.[34] after the magnetic follow-up of nanocubes degradation in intracellular-like conditions. Overall, please also note that a similar dependence of losses per cycle on the field amplitude (panels e,f) can be found in Hergt *et al*.[35] Finally, Fig. 4(g,h) shows a peak in the hysteresis losses as a function of concentration, a behavior reported e. g. by Diamantopoulos *et al*.[36] All together, we have demonstrated that different hyperthermia experiments can be described as particular regions of the general magnetic-hyperthermia scenario depicted in Fig. 3, thus supporting its adequacy as a suitable tool to carry out a comprehensive study of the role of the key-parameters for efficient hyperthermia performance.

Experimental confirmation of non-monotonic heat dissipation. The general character of the results displayed in Fig. 3 may be used not only to understand conflicting results reported in the literature but, more importantly, may serve as a guide for the design of hyperthermia experiments with superior performance. In this regard, the most important feature of the curves displayed in Fig. 3 is the existence of non-monotonic curves with a peak at non-diluted conditions, which stands for optimum heat-dissipation conditions. However, to the best of our knowledge no such trend has been experimentally observed so far. Thus we can make use of the dimensionless character of the general hyperthermia scenario to predict which type of particles (as defined by their K and M_S values) will more likely report the optimizing heat-release features. The particles must display a monotonic decrease of SAR with increasing concentrations for H_{MAX} values of the

order of H_A, and non-monotonic behavior for larger field amplitudes. It is clear that both low H_A and c_0 values are required in order to cover a wide c/c_0 range, with at the same time low H_{MAX}. Good candidates to fulfill those conditions are iron-based nanoparticles, which present moderate M_S and K, and blocking behavior of their magnetic moment at room temperatures and moderate frequencies (i.e. ferromagnetic-like behavior). Recent works have shown that mono-dispersed and crystalline Fe_3O_4 nanoparticles maintain similar M_S values independently of size, while K can be precisely tuning by varying size.[10] Thus, we studied the heating efficiency of magnetite nanoparticles of different size in order to assess their hyperthermia response as a function of H_{MAX} and nanoparticle concentration. We have found that particles with 19 nm in diameter (see Supporting Information) clearly reproduce the general features predicted by the model. Figure 5 shows a non-monotonic behavior of SAR with nanoparticle concentration at given frequency (107 kHz) and different field amplitudes ($\mu_0 H_{MAX}$= 50, 10 and 5 mT). In addition, a clear shift of SAR maximum values is observed towards lower concentrations when decreasing H_{MAX}. The SAR maxima underline the influence of nanoparticle concentration and applied magnetic field on determining their magnetic response. These experimental measurements clearly support the predictive character of our theoretical model shown in Figure 3. Details of the quantitative comparison are described in the Supporting Information, as well as examples for other types of magnetic nanoparticles associated to specific combinations of K and M_S (particularly FeO and Fe).

Theoretical interpretation of the non-monotonic curve. It is important now to gain understanding of the physical origin of the non-monotonic features in Fig. 3 and 5. We interpret this general heat-dissipation scenario in terms of the transition from a single-particle regime to a collective-particle one, and of the transition between major and minor hysteresis loops. We

assume the hysteresis processes are defined by the values of energy barriers as a function of applied fields. In this picture, in order to reverse the magnetization and dissipate energy, a magnetic field large enough as to overcome the local energy barrier felt by each particle must be applied. At low concentrations, the magnetic behavior of the system is single-particle-type, being the energy barrier mainly determined by the anisotropy and Zeeman energies (i.e. negligible HL for $H_{MAX} < 0.5\ H_A$). Increasing interactions (for small concentrations) result in an overall decrease of the anisotropy energy barriers,[37] and thus in a reduction of the HL. Further increase of the concentration drives the system to a collective-particle scenario in which the magnetic behavior of the particles is no longer determined by their individual anisotropy, but it is instead ruled by their coupling with the neighbors. The HL values are in this case mainly determined by the competition between the Zeeman and dipolar energies. The threshold between both individual and collective regimes occurs at the minimum of the high-field curves, at about $c \sim c_0/2$, i.e. when $cM_S^2 < K$ the anisotropy energy dominates over the dipolar one, and the contrary for $cM_S^2 > K$. The collective-particle regime can be understood in terms of a competition between the local dipolar field felt by the particles and the applied field amplitude, as the transition from major to minor loops (see Supporting Information). This competition explains: i) the overlapping of the high-field curves above the minimum, ii) the appearance of the peak, and iii) the HL decay at high concentrations. The above interpretations on the non-monotonic features of the general hyperthermia scenario are schematically illustrated in Figure 6.

Given the generality of the results plotted in Figure 3, in terms of K, M_S, H_{MAX}, and *c*, we propose that the peak in the collective-particle regime may constitute a useful tool to predict optimum conditions for magnetic heating applications.[38] To understand the origin of this peak structure we have carried out a number of calculations, including the average nearest-neighbors

interparticle distance. The results of these calculations indicate that the concentration at which the curves have the maximum (named from now on as c_{opt}) is related to structure-specific features of the ferrofluid (see Supporting Information). On one hand, we have observed a strikingly simple linear dependence of c_{opt} on the field amplitude that can be written as

$$c_{opt} = \frac{2K}{M_S^2}\left(-0.31 + 0.28 H_{MAX}\frac{M_S}{2K}\right), \qquad (1)$$

Applied to the experimental data shown in Figure 5, the predicted optimum concentrations for H_{MAX}=100 Oe, and H_{MAX}=500 Oe, are c_{opt}=0.04 and c_{opt}=0.40, respectively. On the other hand, having in mind the characteristic lengths of biological entities within the tumor tissue it may be interesting to relate this heat-optimizing concentration with the related interparticle distance. Since for the simulations we assumed a liquid-like spatial distribution (likely to resemble a viscous fluid), the equivalent first-nearest-neighbor center to center distance is, in units of the volume fraction, $l_{NN} = (0.445/c)^{1/3}$. Adding this simple relation to equation (1), the equivalent *interparticle distance for optimum hyperthermia* conditions is given by

$$\bar{l}_{opt} = \left(\frac{0.445}{c_0\left(-0.31 + 0.28 H_{MAX}\frac{M_S}{2K}\right)}\right)^{1/3} \qquad (2)$$

For instance, equation (2) estimates that for the case of magnetite nanoparticles as those reported in Fig. 5 the *interparticle distance for optimum hyperthermia* with a field condition of H_{MAX} = 100 Oe is about 2.2 times the particle's diameter. Similarly, we recall Woińska *et al.*[39] calculated that dipole-dipole interactions become rather insignificant for separations exceeding three particle diameters. This regime of interparticle separations may be attained for aggregated particles coated with an organic layer, and could also resemble the situation of most particles

after cellular uptake.[40] Interestingly, the above equation (2) shows some eye-catching similarities with the correlation length of the random anisotropy model (RAM) at high fields,[41] which grows as an inverse power of the field amplitude (although, RAM follows a 1/2 power law). It is important to emphasize, however, the differences between both concepts: the distance described by equation (2) is the average interparticle separation, whereas the RAM correlation length stands for the distance over which a group of magnets behave collectively.

Conclusions. We present a general scenario for the heating performance of magnetic nanoparticles as a function of field amplitude and sample concentration. The model is presented in dimensionless terms able to describe the heating efficiency for any type of magnetic particles under different concentration and field conditions. Concomitantly, we assign the variety of experimental trends reported in the literature to particular regions of this general scenario, demonstrating its usefulness as a tool for the comprehension and design of efficient hyperthermia magnetic seeds and field conditions. Importantly, this scenario also predicts a novel non-monotonic dependence with optimizing-heating features that we have found in magnetite nanoparticles by fine-tuning their anisotropy via size variation. In order to understand such complex scenario we propose a *magnetic hyperthermia trilemma* that rules the magnetic heating performance of nanoparticles as a function of their characteristics, the experimental field settings, and (crucial for the clinical perspective) sample dose. We believe that all together the new findings reported in this work will help in the comprehension of the hyperthermia properties of magnetic nanoparticles and serve as a guide for better clinical conditions.

Materials and methods.

Computational details. We assumed a system of monodisperse particles with random anisotropy axes on a lattice where the nanocrystals are not free to rotate. When magnetic nanoparticles are subjected to an AC magnetic field they show heating effects due to losses during their magnetization reversal process. Apart from the magnetic hysteresis losses, which are the focus of this study, a quite different relaxation path may occur in the case of particles free to oscillate in a fluid. But we note this viscous friction would be suppressed when particles are immobilized in tumor tissue.[6] Thus, we restricted ourselves here to estimate the area (irreversibility) of the hysteresis loop the system undergoes upon the application of the external field. Therefore, the commonly referred to *Specific Absorption Rate* is actually defined as SAR = HL·f energy loss per cycle (HL) times frequency. Calculations were carried out within the standard Metropolis algorithm formalism. The physical model corresponds to the so-called macrospin approximation, in which all the atomic moments rotate coherently and thus an effective macrospin is assigned to each single-domain magnetic nanoparticle. Further, we made the usual assumption that the particles have the simplest case of uniaxial anisotropy and are small enough so that non-uniform magnetization states (domain walls, canting, curling) and Eddy currents are avoided, but at the same time big enough to ensure that superparamagnetism is circumvent (i.e. blocking temperature is above the working temperature).[42] Thus, it is implicit that the thermal energy is much lower than the anisotropy energy. This condition is usually reached experimentally for particles of several tens of nm in diameter under fields of hundreds of kHz in frequency.[20] Clearly, polydispersity may also contribute to the complexity of the magnetic performance but it is beyond the scope of this paper.

The energies governing the magnetic response include the uniaxial anisotropy energy, the magnetostatic energy, and the Zeeman energy, while the exchange-coupling is neglected. Details

on the model used and previous examples on the influence of magnetic interactions on the hysteresis loop calculations can be found in Ref. [13,14,22].

Synthesis and surface modification of magnetite nanoparticles. Fe_3O_4 particles were prepared via thermal decomposition of iron(III) acetyl acetonate (3.53 g, 10 M) in 1-octadecene (100 mL) containing oleic acid (8.47 g, 30 mM) and 1,2-dodecanediol (4.05 g, 20 mM). The experiment resulting in the formation of particles with a mean size of 18 nm, is described as follows: first, the mixture, stirred under a flow of nitrogen under atmospheric pressure, was heated at a constant rate of 2 °C/minute until a temperature about 195-200 °C. The mixture was kept under reaction for 1 hour, and then heated to 295 °C at 0.3 °C/minute. After waiting for 30 minutes, the mixture was allowed to cool down to ambient temperature. The resulting black precipitate was collected by adding excessive ethanol and centrifugation. The precipitate was re-dispersed into toluene. Later, particles (80 ml of 1.8 mM iron in toluene) were transferred to water by ligand exchange using *meso*-2,3-dimercaptosuccinic acid (DMSA) (2 mM) in dimethyl sulfoxide (20 ml), while mechanically stirring for 48 h.[43] Precipitation out of the DMSA solution was done with phosphate buffered saline (PBS). The supernatant was discarded; the pellet was washed three times with ethanol and re-dispersed in distilled water. Finally, this homogeneous dispersion was filtered and sterilized through a 0.22 μm pore-size syringe. For hyperthermia experiments, solutions were adjusted to pH 7 by dropwise addition of NaOH.

Morphology and colloidal characterization. Transmission electron microscopy (TEM) was performed using a 200-keV JEOL-2000 FXII microscope. Particle size, shape and distribution were analyzed from TEM images [See Supporting Information]. Colloidal characterization was performed by dynamic light scattering (DLS) using a ZetaSizer Nano ZS (Malvern). The iron

concentration was determined by inductively coupled plasma atomic emission spectroscopy (ICP-AES).

AC magnetic field experiments. The hyperthermia response of magnetite nanoparticles dispersed in water was determined at 107 kHz by non-adiabatic calorimetric measurements, as described elsewhere.[44] Temperature variations after applying the field were monitored (± 0.2 ºC) via a commercial optical fiber probe TS2/2 connected to a FOTEMP2-16 two-channel signal analyzer from Optocon AG. The methodology for extracting SAR values is based on repeating three times the time variation temperature curves of iron oxide nanoparticle dispersions at given iron mass concentration and field conditions. Thus, we extract the values of the maximal slope at initial times after switching on H_{AC} (i.e., $dT/dt|_{max}$) for determining its average value and standard deviation. Afterward, SAR values are determined by using the expression:

$$SAR = \frac{C_d m_d}{m_{Fe}} \left| \frac{dT}{dt} \right|_{\max} \qquad (3)$$

where C_d is the water specific heat, m_d is the mass dispersion and m_{Fe} is the mass of iron diluted in the sample, $dT/dt\,|_{max}$ is the average value of the maximal slope at initial times after switching on H_{AC}.

AUTHOR INFORMATION

Corresponding Author

*E-mail: ivan.conde@usc.es and david.serantes@icmm.csic.es

Author Contributions

IC-L, DS and CM-B conceived and planned the study, and chiefly wrote the paper, with input from other co-authors. IC-L carried out the simulations with the assistance of DS, OC-F and DB. MPM and GS synthesized the particles, and FJT and DC performed the hyperthermia experiments. All authors discussed the data and commented on the manuscript.

Notes

The authors declare no competing financial interest.

ACKNOWLEDGMENT

We thank the Centro de Supercomputación de Galicia (CESGA) for the computational facilities. This work was partially supported by the EU (projects FEMTOSPIN, Ref. NNP3-SL-2012-281043; and MULTIFUN, Ref. 246479), the Spanish Ministry of Economy and Competitiveness (FIS2010-20979-C02-02, MAT2009-08165, MAT2011-23641, MAT2013-47395-C4-3-R, CONSOLIDER CSD2007-00041), Xunta de Galicia (INCITE 08PXIB236052PR and EM2013/037), and Gobierno de la Comunidad de Madrid (NANOFRONTMAG, S2013/MIT-2850). IC-L (BES-2010-033138) acknowledges financial support from FPI subprogram. CM-B (RYC-2008-02054) and FJT (RYC-2011-09617) acknowledge financial support from the "Ramón y Cajal" subprogram.

REFERENCES

[1] Colombo M.; Carregal-Romero, S.; Casula, M. F.; Gutiérrez, L.; Morales, M. P.; Böhm, I. B.; Heverhagen, J. T.; Prosperi, D.; Parak, W. J. *Chem. Soc. Rev.* **2012**, 41, 4306-4334.

[2] Strebhardt, K.; Ullrich, A. *Nat. Rev. Cancer* **2008**, 8, 473-480.

[3] Moon, E. J.; Sonveaux, P.; Porporato, P. E.; Danhier, P.; Gallez, B.; Batinic-Haberle, I.; Nien, Y.-C.; Schroeder, T.; Dewhirst, M. W. *PNAS.* **2010,** 107, 20477-20482.

[4] Hildebrandt, B.; Wust, P.; Ahlers, O.; Dieing, A.; Sreenivasa, G.; Kerner, T.; Felix, R.; Riess, H. *Crit. Rev. Oncol. Hematol.* **2002**, 43, 33–56

[5] Fernando, R.; Maples, D.; Senavirathna, L. K.; Zheng, Y.; Polf, J. C.; Benton, E. R.; Bartels, K. E.; Piao, D.; Ranjan, A.; *Pharm. Res.* **2014**, 31, 3120.

[6] Dutz, S.; Hergt, R. *Nanotech.* **2014,** 25, 452001.

[7] Mehdaoui, B.; Tan, R. P.; Meffre, A.; Carrey, J.; Lachaize, S.; Chaudret, B.; Respaud, M. *Phys. Rev. B* **2013**, 87, 174419.

[8] Dennis, C. L.; Jackson, A. J.; Borchers, J. A.; Hoopes, P. J.; Strawbridge, R.; Foreman, A. R.; van Lierop, J.; Gruttner, C.; and Ivkov, R. *Nanotech.* **2009,** 20, 395103.

[9] Eggeman, A. S.; Majetich, S. A.; Farrell, D.; and Pankhurst, Q. A. *IEEE Trans. Magn.* **2007,** 43, 2451.

[10] Salas, G.; Camarero, J.; Cabrera, D.; Takacs, H.; Varela, M.; Ludwig, R.; Dahring, H.; Hilger, I.; Miranda, R.; Puerto Morales, M. P.; Teran, F. J. *J. Phys. Chem. C* **2014,** 118, 19985.

[11] Dutz, S.; Clement, J. H,; Eberbeck, D.; Gelbrich, T.; Hergt, R.; Mueller, R.; Wotschadlo, J.; and Zeisberger, M. *J. Magn. Magn. Mater.* **2009,** 321, 1501.

[12] Lartigue, L.; Hugounenq, P.; Alloyeau, D.; Clarke, S. P.; Levy, M.; Bacri, J-C.; Bazzi, R.; Brougham, D. F.; Wilhelm, C.; and Gazeau, F. *ACS Nano* **2012,** 6, 10935.

[13] Serantes, D.; Baldomir, D.; Martinez-Boubeta, C.; Simeonidis, K.; Angelakeris, M.; Natividad, E.; Castro, M.; Mediano, A.; Chen, D.-X.; Sanchez, A.; Balcells, L. I.; Martinez, B. *J. Appl. Phys.* **2010**, 108, 073918.

[14] Martinez-Boubeta, C.; Simeonidis, K.; Serantes, D.; Conde-Leborán, I.; Kazakis, I.; Stefanou, G.; Peña, L.; Galceran, R.; Balcells, L.; Monty, C.; Baldomir, D.; Mitrakas, M.; Angelakeris, M. *Adv. Func. Mater.* **2012**, 22, 3737.

[15] Burrows, F.; Parker, C.; Evans, R. F. L.; Hancock, Y.; Hovorka, O.; Chantrell, R. W. *J. Phys. D : Appl. Phys.* **2010**, 43, 474010.

[16] Haase, C.; Nowak, U. *Phys. Rev. B* **2012**, 85, 045435.

[17] Mamiya, H.; Jeyadevan, B. Sci. Rep. **2011,** 1, 157.

[18] Serantes, D.; Simeonidis, K.; Angelakeris, M.; Chubykalo-Fesenko, O.; Marciello, M.; del Puerto Morales, M.; Baldomir, D.; Martinez-Boubeta, C. *J. Phys. Chem. C,* **2014,** 118, 5927–5934.

[19] Ortega, D.; Pankhurst, Q. A. *Nanoscience* **2013**, 1, 60–88.

[20] Mehdaoui, B.; Meffre, A.; Carrey, J.; Lachaize, S.; Lacroix, L. M. ; Gougeon, M.; Chaudret, B.; Respaud, M. *Adv. Funct. Mater.* **2011**, 21, 4573-4581.

[21] Bertotti, G. *Hysteresis in Magnetism, Academic Press, Boston*, **1998**.

[22] Martinez-Boubeta, C.; Simeonidis, K.; Makridis, A.; Angelakeris, M.; Iglesias, O.; Guardia, P.; Cabot, A.; Yedra, L.; Estradé, S.; Peiró, F.; Saghi, Z.; Midgley, P. A.; Conde-Leborán, I.; Serantes, D.; Baldomir, D. *Sci. Rep.* **2013**, 3, 1652.

[23] Lee, J.-H.; Jang, J.-T.; Choi, J.-S.; Moon, S. H.; Noh, S.-H.; Kim, J.-W.; Kim, J.-G.; Kim, I.-S.; Park, K. I.; Cheon, J. *Nature Nanotech.* **2011**, 6, 418.

[24] Ivkov, R. *Int. J. Hyperthermia* **2013**, 29, 703-705.

[25] Richter, H. J.; Dobin, A. Yu. *J. Magn. Magn. Mater.* **2005**, 287, 41-50.

[26] Jeun, M.; Bae, S.; Tomitaka, A.; Takemura, Y.; Park, K. H.; Paek, S. H.; Chung, K. W. *Appl. Phys. Lett*. **2009**, 95, 082501.

[27] Khot, V. M.; Salunkhe, A. B.; Thorat, N. D.; Phadatare, M. R.; Pawar, S. H. *J. Magn. Magn. Mater.* **2013**, 332, 48.

[28] Beković, M.; Trlep, M.; Jesenik, M.; Goričan, V.; Hamler, A. *J. Magn. Magn. Mater.* **2013**, 331, 264.

[29] Landi, G. T.; Bakuzis, A. F. *J. Appl. Phys.* **2012**, 111, 083915.

[30] Usov, N. A. *J. Appl. Phys.* **2010**, 107, 123909.

[31] Cervadoro, A.; Giverso, C.; Pande, R.; Sarangi, S.; Preziosi, L.; Wosik, J.; Brazdeikis, A.; Decuzzi, P. *PLoS ONE* **2013**, 8, e57332.

[32] Meffre, A.; Mehdaoui, B.; Kelsen, V.; Fazzini, PF.; Carrey, J.; Lachaize, S.; Respaud, M.; Chaudret, B. *Nano Lett.* **2012**, 12, 4722-4728.

[33] De Sousa, M. E.; van Raap, M. B. F.; Rivas, P. C.; Zélis, P. M.; Girardin, P.; Pasquevich, G. A.; Alessandrini, J. L.; Muraca, D.; Sánchez, F. H. *J. Phys. Chem. C* **2013**, 117, 5436.

[34] L. Lartigue, L.; Alloyeau, D.; Kolosnjaj-Tabi, J.; Javed, Y.; Guardia, P.; Riedinger, A.; Péchoux, C.; Pellegrino, T.; Wilhelm, C.; Gazeau, F. *ACS Nano* **2013,** 7, 3939–3952.

[35] Hergt, R.; Dutz, S.; Müller, R.; Zeisberger, M. *J. Phys. Condens. Matter* **2006**, 18, S2919.

[36] Diamantopoulos, G.; Basina, G.; Tzitzios, V.; Karakosta, E.; Fardis, M.; Jagličić, Z.; Lazaridis, N.; Papavassiliou, G. *J. Magn. Magn. Mater.* **2013**, 336, 71.

[37] Abbasi, A. Z.; Gutierrez, L.; del Mercato, L. L.; Herranz, F.; Chubykalo-Fesenko, O.; Veintemillas-Verdaguer, S.; Parak, W. J.; Morales, M. P.; Gonzalez, J. M.; Hernando, A.; de la Presa, P. *J. Phys. Chem. C* **2011**, 115, 6257.

[38] Note that we refer here to optimizing conditions as those corresponding to maximum heating power *per sample volume*. For applications it should be also taken into account the fact that very diluted samples, even if dissipate large energy per particle, will result in very low heat release *per volume of tumour tissue*. This is illustrated in the Supporting Information, Fig. S7.

[39] Woińska, M.; Szczytko, J.; Majhofer, A.; Gosk, J.; Dziatkowski, K.; and Twardowski, A. *Phys. Rev. B* **2013,** 88, 144421.

[40] Kolosnjaj-Tabi, J.; Di Corato, R.; Lartigue, L.; Marangon, I.; Guardia, P.; Silva, A. K. A.; Luciani, N.; Clément, O.; Flaud, P.; Singh, J. V.; Decuzzi, P.; Pellegrino, T.; Wilhelm, C.; Gazeau, F. *ACS Nano* **2014,** 8, 4268-4283.

[41] Chudnovsky, E.M. *J. Appl. Phys.* **1988,** 64, 5770.

[42] Serantes, D.; Baldomir, D.; Pereiro, M.; Hoppe, C. E.; Rivadulla, F.; Rivas, J. *Phys. Rev. B* **2010**, *82*, 134433.

[43] Salas, G.; Casado, C.; Teran, F. J., Miranda, R. ; Serna, C. J.; Morales, M.P. *J. Mater. Chem.*, **2012**, *22*, 21065.

[44] Teran, F. J.; Casado, C.; Mikuszeit, N.; Salas, G.; Bollero, A.; Morales, M. P.; Camarero, J.; Miranda, R. *Appl. Phys. Lett.* **2012**, *101*, 062413.

FIGURES

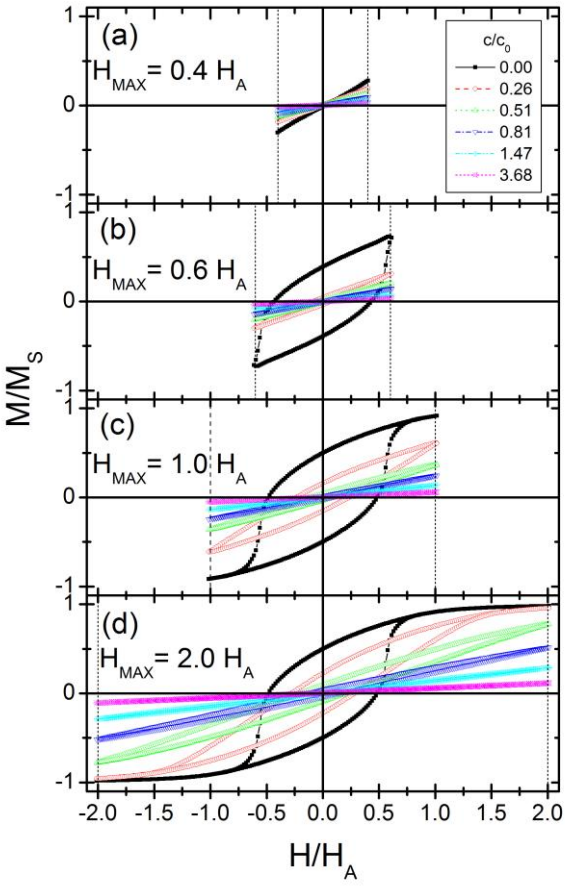

Fig. 1. Influence of interaction conditions (depicted as increasing c/c_0 values) on hysteresis losses for different field amplitudes H_{MAX} (see text for details). Stoner–Wohlfarth non-interacting particles are represented by the case $c/c_0 = 0$.

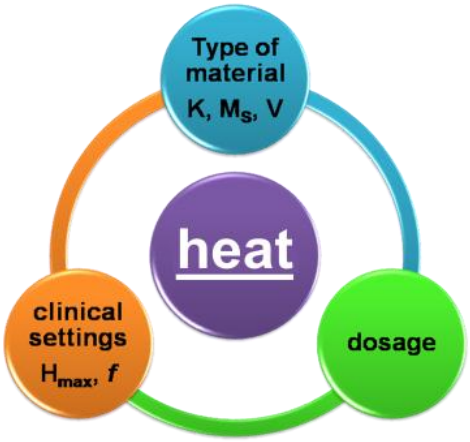

Fig. 2. Schematic illustration of the *magnetic hyperthermia trilemma*, which describes problem associated with reconciling nanoparticles attributes with appropriate concentration without sacrificing heat conversion while maintaining affordable field generator conditions.

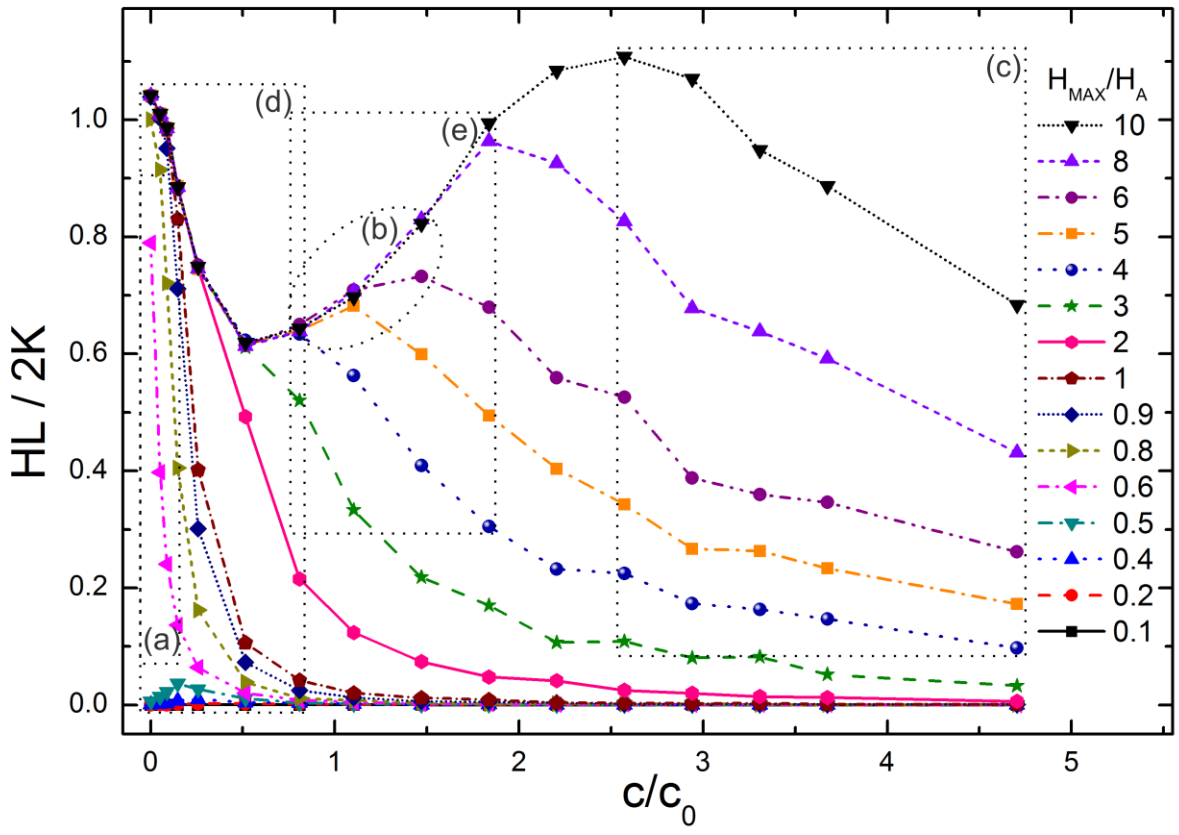

Fig. 3. *Dimensionless magnetic-hyperthermia scenario*. Computation results of heating efficiency (HL/2K) *vs.* sample concentration (c/c_0) for different field amplitudes (H_{MAX}/H_A).

Dashed regions account for diverse heating behaviours (detailed in Fig. 4): (a,c) describe a decrease in heating power when the concentration increases, while (b) exhibits an increase, and within (e) both tendencies are present as a function of the intensity of the applied field.

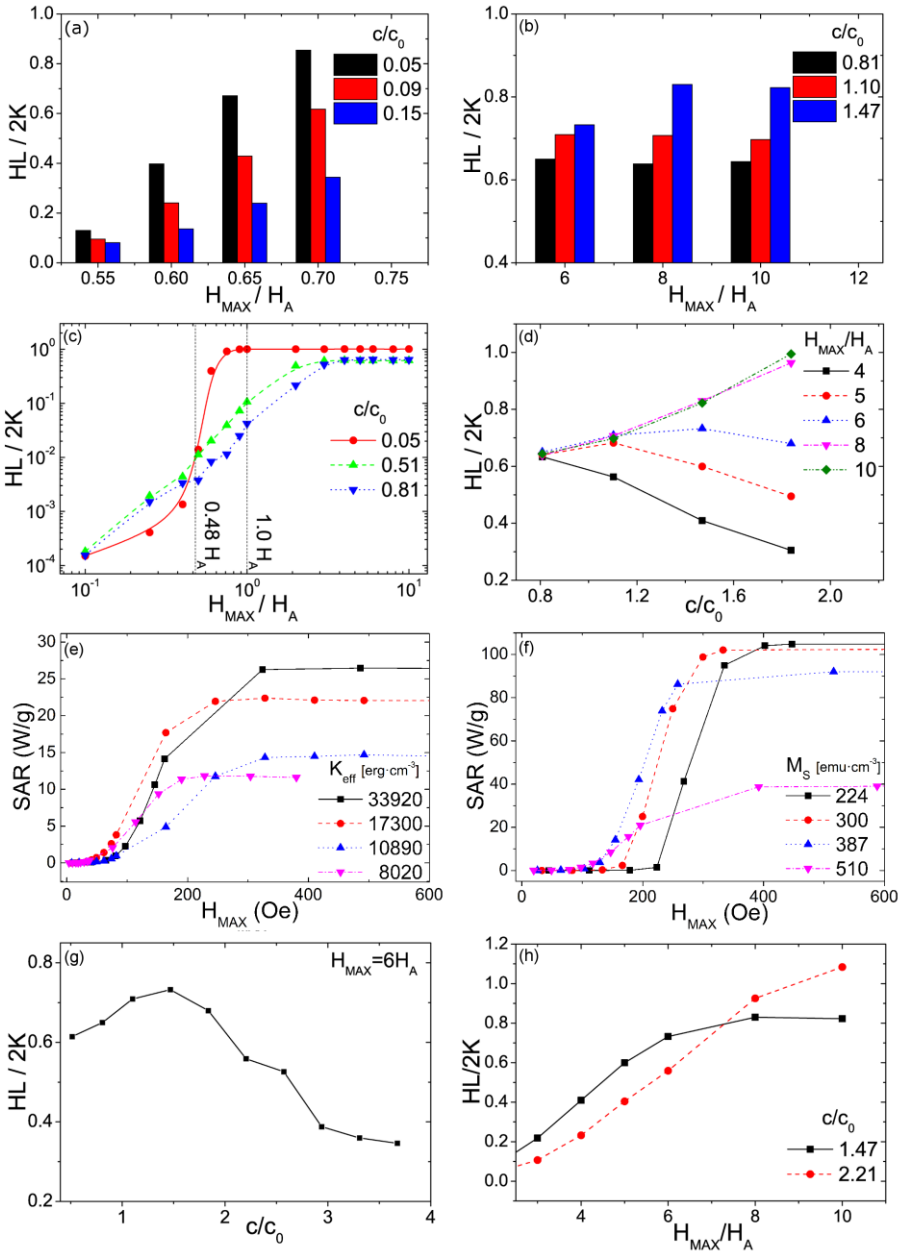

Fig. 4. Heating efficiency trends derived from the model predictions displayed in Fig. 3. Graphs (a-h) provide conditions easily comparable to experimental trends reported in the literature (see text for a detailed discussion).

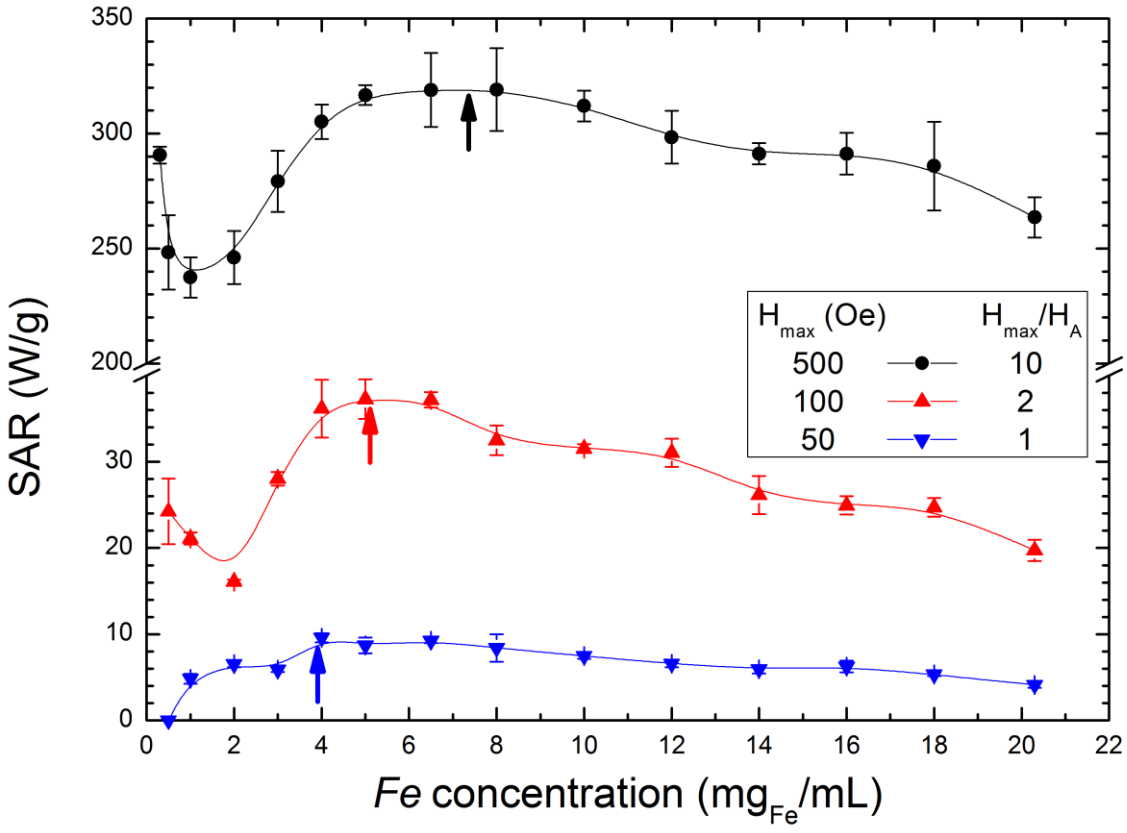

Fig. 5. *Experimental confirmation* of the non-monotonic concentration dependence of heating efficiency with optimum heating features. The symbols are the experimental data on the iron concentration dependence of the SAR values for magnetite colloids, at different H_{MAX} and given

frequency (107 kHz). Arrows depict the concentration value at which SAR value is maximum for each H_{MAX}.

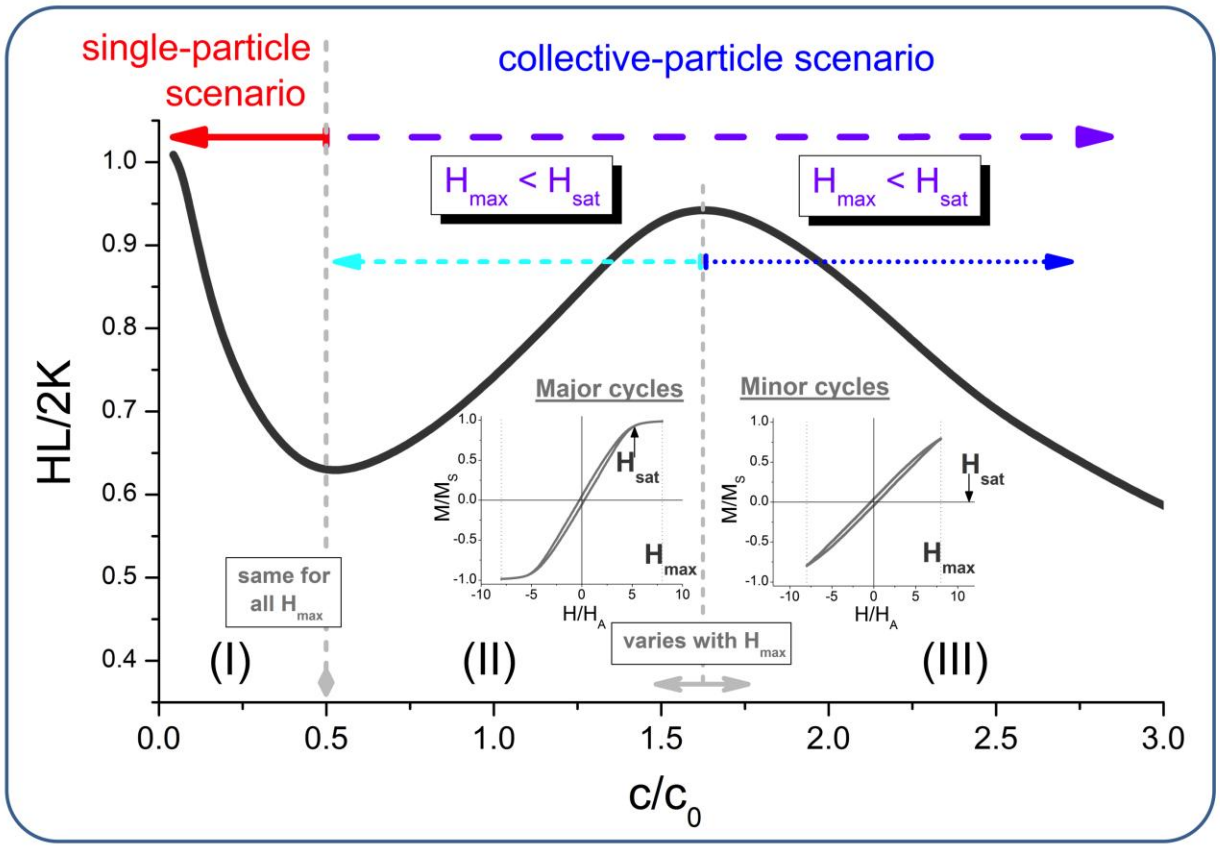

Fig. 6. *Schematic description of the magnetic-hyperthermia scenario.* Dependency of magnetic properties on packing density (see Fig. 3). The transition from single particle to collective behavior with increasing volume concentration is discussed as a function of the magnetic anisotropy. Range (I) corresponds to the *single-particle* scenario, in which the particles' response is determined by their magnetic anisotropy and whereas hysteresis losses decay upon increasing c. Ranges (II) and (III) correspond to the *collective-particle* scenario, in which the system response is determined by the interparticle coupling. The threshold between the single-particle

and collective-particle scenarios occurs at the minimum of the curves at about $c/c_0 \approx 0.5$, and is independently of the applied field. On the opposite, the maximum signals the concentration at which the field is not longer enough to saturate the sample, and therefore scales at higher concentrations for larger fields.